A general time-dependent stochastic method for solving Parker's transport equation in spherical coordinates

C. Pei,[1] J. W. Bieber,[1] R. A. Burger,[2] and J. Clem[1]

Received 26 May 2010; revised 10 September 2010; accepted 28 September 2010; published 11 December 2010.

[1] We present a detailed description of our newly developed stochastic approach for solving Parker's transport equation, which we believe is the first attempt to solve it with time dependence in 3-D, evolving from our 3-D steady state stochastic approach. Our formulation of this method is general and is valid for any type of heliospheric magnetic field, although we choose the standard Parker field as an example to illustrate the steps to calculate the transport of galactic cosmic rays. Our 3-D stochastic method is different from other stochastic approaches in the literature in several ways. For example, we employ spherical coordinates to integrate directly, which makes the code much more efficient by reducing coordinate transformations. What is more, the equivalence between our stochastic differential equations and Parker's transport equation is guaranteed by Ito's theorem in contrast to some other approaches. We generalize the technique for calculating particle flux based on the pseudoparticle trajectories for steady state solutions and for time-dependent solutions in 3-D. To validate our code, first we show that good agreement exists between solutions obtained by our steady state stochastic method and a traditional finite difference method. Then we show that good agreement also exists for our time-dependent method for an idealized and simplified heliosphere which has a Parker magnetic field and a simple initial condition for two different inner boundary conditions.

Citation: Pei, C., J. W. Bieber, R. A. Burger, and J. Clem (2010), A general time-dependent stochastic method for solving Parker's transport equation in spherical coordinates, *J. Geophys. Res.*, *115*, A12107, doi:10.1029/2010JA015721.

1. Introduction

[2] Solar modulation is the process by which the Sun impedes the entry of galactic cosmic rays into the solar system, thereby altering the intensity and energy spectrum of the cosmic rays. Understanding solar modulation from first principles is a challenging astrophysical problem, because it requires an understanding of the properties of magnetic fields and turbulence throughout the heliosphere, while also demanding accurate theories for determining particle transport properties, such as the diffusion tensor, from the properties of the turbulence.

[3] A comprehensive understanding of solar modulation is required for extracting information about extrasolar phenomena from observations of charged cosmic rays made within the heliosphere. For instance, consideration of modulation effects is crucial for interpreting time variations of the antiproton/proton ratio [*Bieber et al.*, 1999; *Mitchell et al.*, 2008]. Solar modulation effects must also be considered for mitigation of radiation hazard from galactic cosmic rays, both for astronauts on long-duration deep space missions, and for sensitive electronic components flown in space. The significance of modulation effects is highlighted by recent observations that the intensity of galactic cosmic rays in the inner heliosphere has risen to a new space age high [*Mewaldt et al.*, 2009].

[4] The governing equation for solar modulation is Parker's well-known transport equation [*Parker*, 1965; *Jokipii and Parker*, 1970],

$$\frac{\partial f}{\partial t} = \nabla \cdot (\boldsymbol{\kappa} \cdot \nabla f - \mathbf{V} f) + \frac{1}{3p^2}(\nabla \cdot \mathbf{V})\frac{\partial p^3 f}{\partial p}, \qquad (1)$$

where $f(\mathbf{r}, p, t)$ is the omni-directional distribution function (i.e., the phase space density averaged over solid angle in momentum space), with p the particle momentum, $\mathbf{r}$ the spatial variable and $\mathbf{V}$ the solar wind velocity. Note that we drop the subscript 0 typically used for the omni-directional distribution function. Terms relating to the second-order Fermi acceleration and sources will not be discussed in this paper. The spatial diffusion tensor, $\boldsymbol{\kappa}$, can be decomposed into two parts, $\boldsymbol{\kappa}_s$, the symmetric part, and $\boldsymbol{\kappa}_A$, the antisymmetric part. The divergence of the antisymmetric tensor, $\boldsymbol{\kappa}_A$, is the drift velocity, $\mathbf{V}_d$. The symmetric tensor, $\boldsymbol{\kappa}_s$, consists of the spatial diffusion parallel $\kappa_{\|}$ and perpendicular

[1]Bartol Research Institute, Department of Physics and Astronomy, University of Delaware, Newark, Delaware, USA.
[2]Unit for Space Physics, School of Physics, North-West University, Potchefstroom, South Africa.

0148-0227/10/2010JA015721

$\kappa_\perp$ to the mean heliospheric magnetic field, **B**, which is given by

$$\mathbf{B} = \frac{A}{r^2}\left(\hat{\mathbf{e}}_r - \frac{(r - r_\odot)\Omega_\odot}{V}\sin\theta\hat{\mathbf{e}}_\phi\right)\left[1 - 2H\left(\theta - \frac{\pi}{2}\right)\right], \quad (2)$$

where $A = \pm B_{0r} r_0^2$ is a constant which comes from the definition of the magnetic field, with suffix 0 indicating some reference value and the sign depending on solar cycle, and $\Omega_\odot$ is the sidereal solar rotation rate corresponding to a period of 25.4 days. The radius from which the field is purely radial is denoted by $r_\odot$ which is usually several times the solar radius although we take it to be 0 for the benchmarking against the finite difference method. The Heaviside step function is represented by H. Please note that equation (2) is only for a heliospheric magnetic field with a flat neutral sheet. Although our method presented here is also applicable to a wavy neutral sheet, it is too complicated to discuss here.

[5] The parallel diffusion component with respect to the magnetic field, $\kappa_\parallel$, and the perpendicular component, $\kappa_\perp$, can be determined *ab initio* from turbulence models based on spacecraft measurements [see, e.g., *Pei et al.*, 2010]. In this paper, however, we choose three ad hoc analytical forms for $\kappa_\parallel$ in order to simplify our benchmark procedure; we leave *ab initio* models for future publication. These forms are

$$\kappa_\parallel = \kappa_0 \beta P \frac{B_e}{B}, \quad (3)$$

$$\kappa_\parallel = \kappa_0 \beta P (1 + 0.5\sin\phi)\frac{B_e}{B}, \text{or} \quad (4)$$

$$\kappa_\parallel = \kappa_0 \beta P [1 + 0.8\sin(\Omega t)] (\text{alternative version for time dependence}), \quad (5)$$

$$\kappa_\perp / \kappa_\parallel = 0.1, \quad (6)$$

where P is the particle rigidity, κ_0 is a constant, β is the ratio between particle speed and the speed of light, B is the magnetic field magnitude with B_e its value at the Earth, and ϕ is the azimuth angle in a heliocentric spherical coordinate system. The first two forms are for the benchmark of steady state solutions. The third one is for the benchmark of time-dependent solutions. Note that with Parker's magnetic field, $\boldsymbol{\kappa}$ is a function of only (r, θ) in equation (4) which is not a fully 3-D function. In equation (5), $\boldsymbol{\kappa}$ is a function of (r, θ, ϕ).

[6] Two major numerical methods have been developed to solve equation (1). One is the finite difference method, a deterministic method, employed by, e.g., *Jokipii and Kopriva* [1979], *Potgieter and Moraal* [1985], and *Burger and Hattingh* [1995]. In order to benchmark our new method, a steady state three-dimensional finite difference method [*Burger and Hattingh*, 1995], following the approach of *Kóta and Jokipii* [1983], is used in this paper. The other major method is the stochastic or Monte Carlo method used by *Jokipii and Owens* [1975], *Jokipii and Levy* [1977], *Yamada et al.* [1998], *Zhang* [1999a, 1999b], *Gervasi et al.* [1999], *Miyake and Yanagita* [2005], *Ball et al.* [2005], *Alanko-Huotari et al.* [2007], *Bobik et al.* [2008], *Alanko-Huotari et al.* [2009], and *Pei et al.* [2009]. For 1-D and 2-D problems, the finite difference method is much faster than the stochastic method. However, for fully 3-D and energy-dependent problems and for a complex heliospheric magnetic field, for example, if we consider the wavy current sheet and the time-dependent problem, the stochastic method is promising because we don't have a successful finite difference method for this situation so far. In this paper we provide a direct comparison between the results of these two methods for different scenarios.

[7] One big advantage of the stochastic method is that it is very easy to parallelize so that it can be running on many CPUs of a local cluster, with almost unchanged codes. Due to the nature of this method with each random process independent of all others, it can also be very easily adjusted to be running on distributed idle computers which can reduce the computation time and lower the hardware costs dramatically. Although this method has been investigated by many research groups in the past, most efforts are focused on finding the steady state solutions of equation (1). As far as we know, no 3-D time-dependent stochastic method has been published although some work has been done for the 1-D time-dependent case [*Yamada et al.*, 1999; *Li et al.*, 2009]. In this paper we present our time-dependent method with a discussion of the initial conditions and boundary conditions.

[8] In a related problem, the stochastic method has also been applied to solve Roelof's Equation [*Roelof*, 1969], which usually is used to describe the transport of solar energetic particles with significant anisotropies [*Kocharov et al.*, 1998; *Zhang et al.*, 2009; *Dröge et al.*, 2010]. The 3-D stochastic method introduced by *Zhang et al.* [2009] and *Dröge et al.* [2010] is applied to a modified Roelof's Equation which includes the transport mechanisms of streaming, convection, pitch angle diffusion, focusing, perpendicular diffusion, and pitch angle–dependent adiabatic cooling. This method can be easily adjusted to arbitrary magnetic field geometries and to transport parameters that vary spatially as well as with energy.

[9] Our method described in the present manuscript is completely adequate for the application discussed here, i.e., the solar modulation of galactic cosmic rays. Further, the method based upon Parker's equation optimizes the computing time required to achieve the necessary accuracy in modulation applications. It differs from the others in several additional ways.

[10] 1. We present every step in great detail to reproduce our results in this paper including the step transforming the original Parker's equation to the standard Fokker-Planck equation. This step has been omitted mostly in literature but we believe it is important when the diffusion coefficient is not a constant (see Appendix C) in 3-D models.

[11] 2. We use spherical coordinates which is convenient to use, for example, easy to specify boundary conditions and the magnetic field while most other 3-D methods [*Zhang*, 1999b; *Ball et al.*, 2005] use Cartesian coordinates. *Zhang* [1999b] states that the integration of stochastic differential equations must be performed in terms of Cartesian coordinates. We show, however, that for a general form for the heliospheric magnetic field, we can actually use spherical coordinates directly. A more detailed discussion can be found in section 2.

[12] 3. Our steady state results are strictly benchmarked with the traditional finite difference solutions with the same set of parameters. Our time-dependent solutions are bench-

marked by Mathematica with the same boundary conditions and initial conditions. The benchmarking results are presented in section 3.

2. Stochastic Method

[13] The stochastic method to solve equation (1) can be divided into two steps which will be illustrated in detail in this section from 1-D to 3-D. The first step is that we need to find the corresponding SDEs to equation (1) based on Ito formula and solve it. The second step is that we obtain the modulated distribution function from the solutions of the corresponding SDEs.

[14] To find the corresponding SDEs, it is convenient to transform equation (1) into the standard form of the Fokker-Planck equation (FPE),

$$\frac{\partial F}{\partial t} = -\sum_i \frac{\partial}{\partial q_i}[A_i(\mathbf{q},t)F] + \frac{1}{2}\sum_{i,j}\frac{\partial^2}{\partial q_i \partial q_j}\left\{\left[\mathsf{B}(\mathbf{q},t)\mathsf{B}^T(\mathbf{q},t)\right]_{i,j}F\right\}, \tag{7}$$

where $\mathbf{A}$ is a vector (though often termed the drift vector in discussions of the stochastic method, it is not the same as the drift velocity, $\mathbf{V}_d$), and $\mathsf{D} = \mathsf{B}\mathsf{B}^T$ is the diffusion tensor [*Gardiner*, 2004]. Note that this B is not the magnetic field $\mathbf{B}$. Moreover, here q_i denotes a generalized vector with both spatial and momentum or energy components. The general form for $\mathbf{A}$ is $(A_r, A_\theta, A_\phi, A_p)$. The general form for B is a four by four matrix generally,

$$\mathsf{B} = \begin{bmatrix} \mathsf{B}_{rr} & \mathsf{B}_{r\theta} & \mathsf{B}_{r\phi} & \mathsf{B}_{rp} \\ \mathsf{B}_{\theta r} & \mathsf{B}_{\theta\theta} & \mathsf{B}_{\theta\phi} & \mathsf{B}_{\theta p} \\ \mathsf{B}_{\phi r} & \mathsf{B}_{\phi\theta} & \mathsf{B}_{\phi\phi} & \mathsf{B}_{\phi p} \\ \mathsf{B}_{pr} & \mathsf{B}_{p\theta} & \mathsf{B}_{p\phi} & \mathsf{B}_{pp} \end{bmatrix}.$$

Since second-order acceleration mechanisms are not considered, this matrix can be downgraded to a three by three matrix, i.e., the fourth row and the fourth column can be omitted. This is the case for Appendix B and Appendix C. The specific forms of $\mathbf{A}$ and B and the method to derive them will be provided later in this section for 1-D and 2-D methods. For simplicity, the corresponding 3-D forms and formulas are put in Appendix B and Appendix C.

[15] The equivalent Ito stochastic differential equation is

$$\Delta\mathbf{q} = \mathbf{A}(\mathbf{q},t)\Delta t + \mathsf{B}(\mathbf{q},t)\cdot\Delta\mathbf{W}, \tag{8}$$

which can be solved to provide the normalized transition probability function $G(\mathbf{r}, p, t|\mathbf{r}_e, p_e, t_e)$. The normalization of a general transition probability function is

$$\int\int_\Omega\int G(\mathbf{r},p,t|\mathbf{r}_e,p_e,t_e)dpd^3\mathbf{r}dt = 1, \tag{9}$$

where Ω denotes the whole domain in space. G can also be interpreted as a Green's function [see, e.g., *Webb and Gleeson*, 1977; *Li et al.*, 2009]. Here $\Delta\mathbf{W}$ denotes a Wiener process (see Appendix A). The suffix e denotes the Earth or any location in heliosphere we are interested in. So the process to find the corresponding set of SDEs is the process to determine $\mathbf{A}$, $\Delta\mathbf{W}$, and B. For a general heliospheric magnetic field, the matrix B can be calculated according to Appendix B. In this paper, we focus on the form of B for Parker field which is shown in Appendix C. We show the values of $\mathbf{A}$ and $\Delta\mathbf{W}$ for 1-D and 2-D in section 2.1 and section 2.2. For 3-D, the values of $\mathbf{A}$ and $\Delta\mathbf{W}$ are detailed in Appendix C.

[16] For all the cases, the procedures to integrate the SDEs are similar. First, we start from some initial position, chosen to be the Earth in this paper, $\mathbf{r}_e$, and some initial time, t_e, integrate along the trajectory of the *pseudoparticle*, follow them back in time until they reach the boundary. The backward-in-time integration is more efficient than the forward-in-time approach because it reduces the number of useless pseudo-particles although they are equivalent to each other [*Kóta*, 1977]. A pseudoparticle is not a real particle nor a test particle, but a point in phase space. A real particle or a test particle moves around in the planetary field obeying Lorentz equation and following field lines [*Pei et al.*, 2006]. A pseudoparticle has a tendency to follow field lines according to equation (8) provided that parallel diffusion dominates, but it does not in general follow them rigorously owing to the random Wiener process present in the equation. Then we start the whole process again for another pseudoparticle. In this way, we have the steady state solution for all the pseudoparticles. Because this is equivalent to set $t \to \infty$, we don't need and shouldn't specify the initial condition. In other words, the initial condition has no contribution to our solution. This can also be verified by the missing of time integral in equation (10). For the time-dependent solution, we follow the pseudoparticle to a certain value of t_e which is not equal to infinity. The normalized probability function, $G(\mathbf{r}, p, t|\mathbf{r}_e, p_e, t_e)$, then is calculated based on the trajectories we collected. Normalized probability function, G, is subject to the normalization condition that G integrated over $\mathbf{r}$ and p is unity (see equation 9).

[17] The set of equations in the first step is the same for both steady state solutions and for time-dependent solutions. However, for the second step, we must treat them differently to determine the modulated distribution function.

[18] The modulated distribution function, $f(\mathbf{r}_e, p_e)$, if we just need the steady state solution, is determined by

$$f(\mathbf{r}_e,p_e) = \oint_{\mathbf{r}\in S}\int f_b(\mathbf{r},p)G(\mathbf{r},p|\mathbf{r}_e,p_e)dpda, \tag{10}$$

where S denotes the boundaries which generally are closed surfaces of a multiply connected domain and f_b denotes boundary conditions. A multiply connected domain can be used to take into account of sources like Jupiter.

[19] Equation (10) is a general form for steady state solutions and for general boundaries. If the outer boundary condition is independent of position, the integral over the outer boundary of $G(\mathbf{r}, p|\mathbf{r}_e, p_e)$ gives $G'(p|\mathbf{r}_e, p_e)$ due to the normalization, i.e., $G'(p|\mathbf{r}_e, p_e) = \oint_{\mathbf{r}\in S} G(\mathbf{r}, p|\mathbf{r}_e, p_e)da$. For simplicity, we drop the prime. Thus if at the same time, the inner boundary is a reflecting boundary or an absorbing boundary, equation (10) reduces to

$$f(\mathbf{r}_e,p_e) = \int f_{outer}(p)G(p|\mathbf{r}_e,p_e)dp, \tag{11}$$

which is a 3-D generalization of *Yamada et al.* [1998, equation 6] or *Li et al.* [2009, equation 8], which both are for 1-D and for special inner boundaries only. Another point in equation (11) is that as long as the boundary condition is independent of position, we don't need to know the details

of the final positions of "pseudo" particles on that boundary for any shape of the boundary. For example, even if the heliosphere has an irregular shape, such as a bullet shape, it is sufficient to know the pseudoparticle momentum when it encounters the boundary (traced backward from the Earth). Thus the integral in equation (11) can be computed directly, with no need to form the complicated function $G(\mathbf{r}, p|\mathbf{r}_e, p_e)$ as an intermediate step.

[20] The time-dependent modulated distribution function, $f(\mathbf{r}_e, p_e, t_e)$, in a time-dependent case is determined by

$$f(\mathbf{r}_e,p_e,t_e)=\int_0^{t_e}\oint_{\mathbf{r}\in S(t)}\int f_b(\mathbf{r},p,t)G(\mathbf{r},p,t|\mathbf{r}_e,p_e,t_e)dpdadt + \int\int f_i(\mathbf{r},p,0)G_i(\mathbf{r},p,0|\mathbf{r}_e,p_e,t_e)dpd^3\mathbf{r}, \quad (12)$$

where $f_i(\mathbf{r}, p, 0)$ is the initial condition. An area element on the spatial surface is denoted by da. The integral involving f_i generally is a volume integral in 3-D. The integral involving f_b takes into account of a time-dependent boundary condition which is why we have the integral in time. The time-dependent boundary is important in dealing with solar energetic particles and in taking account of Jovian electrons. G_i is the Green's function for the initial condition which has a different unit from G. So generally speaking, after we obtained the probability function, $G(\mathbf{r}, p, t|\mathbf{r}_e, p_e, t_e)$, from the SDEs, we need to integrate in time, in momentum, and in position over the boundary surface, to get the distribution function we want.

[21] For a time-dependent distribution function, $f(\mathbf{r}_e, p_e, t)$, we choose an arbitrary time interval, Δt_i, which satisfies $V\Delta t_i \ll \sqrt{\kappa\Delta t_i}$, then integrate the SDEs for each term in the time series, $t_i = t_{i-1} + \Delta t_i$. In order to integrate equation (12), we also need to specify an appropriate initial condition for the time-dependent solution, unlike the steady state case where an initial condition is not needed.

[22] In reality, this initial condition should be specified based on observations. In this paper, for the purpose of demonstrating our point, we take the initial condition as

$$f_i(0.01\mathrm{AU} < r < 100\mathrm{AU}, \theta, \phi, p, 0) = 0. \quad (13)$$

This initial condition means initially at $t = 0$ the heliosphere is empty which implies the second integral in equation (12) vanishes. Note that the initial condition of an empty heliosphere is different from no initial condition. At the same time, if we use the same boundaries as we have in the steady state solution case, the first integral in equation (12) can also be simplified in the same way as in equation (11). Taking all these assumptions into account, equation (12) becomes

$$f(\mathbf{r}_e,p_e,t_e)=\int_0^{t_e}\int f_{outer}(p)G(p,t|\mathbf{r}_e,p_e)dpdt. \quad (14)$$

[23] In this paper, we use two types of inner boundary conditions. The first one is the reflecting boundary, namely, $\partial f/\partial r = 0$. The second one is the absorbing boundary, $f = 0$ [*Chandrasekhar*, 1943]. For simplicity we take the local interstellar intensity for protons at 100 AU, j_T^{LIS}, as

$$j_T^{LIS}=\frac{21.1T^{-2.8}}{1+5.85T^{-1.22}+1.18T^{-2.54}}\left(\mathrm{sr\ m^2\ s\ MeV}\right)^{-1}, \quad (15)$$

where T is the kinetic energy in GeV[*Webber and Higbie*, 2003]. This intensity is related to the omni-directional distribution function by $j_T = p^2 f$. To illustrate how to use our stochastic method in detail, we solve equation (1) in 1-D, 2-D, and 3-D step by step in sections 2.1, 2.2, and 2.3, respectively.

2.1. One-Dimensional Stochastic Method

[24] For completeness, we will illustrate the stochastic method solving equation (1) in 1-D, 2-D, and 3-D. The 1-D Parker's transport equation is

$$\frac{\partial f}{\partial t}=\frac{1}{r^2}\frac{\partial}{\partial r}\left(r^2\kappa_{rr}\frac{\partial f}{\partial r}\right)+\frac{1}{3r^2}\frac{\partial}{\partial r}\left(r^2V\right)\frac{1}{p^2}\frac{\partial}{\partial p}\left(p^3f\right) - \frac{1}{r^2}\frac{\partial}{\partial r}\left(r^2Vf\right), \quad (16)$$

where r is the spatial variable, κ_{rr} the radial diffusion coefficient.

[25] In order to find the corresponding set of SDEs, it is convenient to transform equation (16) into the standard form (equation (7)) which can be achieved by setting $F = r^2 f$ for this 1-D problem. Thus equation (16) can be rewritten as

$$\frac{\partial F}{\partial t}=-\frac{\partial}{\partial r}\left[\left(V+\frac{1}{r^2}\frac{\partial r^2\kappa_{rr}}{\partial r}\right)F\right]-\frac{\partial}{\partial p^3}\left(-\frac{1}{r^2}\frac{\partial r^2V}{\partial r}p^3F\right) + \frac{\partial^2}{\partial r^2}\left(\kappa_{rr}F\right), \quad (17)$$

which is in a standard form. Recognizing $\Delta p^3 = 3p^2\Delta p$, setting

$$\mathbf{q} = \{r, p\}, \quad (18)$$

$$\mathbf{A}=\left\{\frac{1}{r^2}\frac{\partial r^2\kappa_{rr}}{\partial r}+V, -\frac{p}{3r^2}\frac{\partial r^2V}{\partial r}\right\}, \quad (19)$$

$$\Delta\mathbf{W}=\sqrt{\Delta t}\{dw_r, 0\}, \quad (20)$$

where $\Delta\mathbf{W}$ is a Wiener process given by the standard normal distribution, dw_r, with a mean of zero and a standard deviation of one which is discussed in more detail in Appendix A, and

$$\mathsf{B}=\begin{bmatrix}\sqrt{2\kappa_{rr}} & 0\\ 0 & 0\end{bmatrix}, \quad (21)$$

we obtain the corresponding SDEs following from equation (8),

$$\Delta r=\left(\frac{1}{r^2}\frac{\partial r^2\kappa_{rr}}{\partial r}+V\right)\Delta t+\sqrt{2\kappa_{rr}\Delta t}dw_r, \quad (22)$$

$$\Delta p=-\frac{p}{3r^2}\frac{\partial r^2V}{\partial r}\Delta t. \quad (23)$$

[26] To find the steady state solution, we integrate the SDEs approximately to $t \to \infty$. Usually, this can be done by choosing a large value for time, say, 1 year for 10 MeV protons. The modulated distribution function $f(r_e, p_e)$ at r_e = 1 AU and at $p = p_e$, is determined by equation (10) or equation (11). For the time-dependent solution, we integrate

the SDEs to a fixed time, t_e. The time-dependent modulated distribution function $f(r_e, p_e, t_e)$ at $r_e = 1$ AU and at $p = p_e$, is determined by equation (12) or equation (14). We will repeat this again for 2-D and 3-D in this paper since this procedure is the same for 2-D and 3-D.

2.2. Two-Dimensional Stochastic Method

[27] For simplicity and for the purpose of benchmarking, let us discuss the 2-D stochastic method without considering drift and cross terms of $\boldsymbol{\kappa}$ which have been ignored in many papers. With these simplifications, according to equation (1), the 2-D transport of cosmic rays in the heliosphere is,

$$\frac{\partial f}{\partial t} = \frac{1}{r^2}\frac{\partial}{\partial r}\left(r^2\kappa_{rr}\frac{\partial f}{\partial r}\right) + \frac{1}{r^2\sin\theta}\frac{\partial}{\partial\theta}\left(\kappa_{\theta\theta}\sin\theta\frac{\partial f}{\partial\theta}\right) + \frac{1}{r^2}\frac{\partial}{\partial r}\left(r^2V\right)\frac{\partial}{\partial p^3}\left(p^3 f\right) - \frac{1}{r^2}\frac{\partial}{\partial r}\left(r^2 V f\right), \tag{24}$$

with (r, θ) the spatial variables in polar coordinates.

[28] Just as in the 1-D case, it is necessary to transform equation (24) to the standard form given in equation (7). In the literature, there are two different ways to do that. For example, by defining $\mu = \cos\theta$, the FPE is

$$\frac{\partial f}{\partial t} = \frac{1}{r^2}\frac{\partial}{\partial r}\frac{\partial}{\partial r}\left(r^2\kappa_{rr} f\right) - \frac{1}{r^2}\frac{\partial}{\partial r}\left(f\frac{\partial r^2\kappa_{rr}}{\partial r}\right) + \frac{\partial}{\partial\mu}\frac{\partial}{\partial\mu} \cdot \left[\left(1-\mu^2\right)\frac{\kappa_{\theta\theta}}{r^2} f\right] - \frac{\partial}{\partial\mu}\left\{f\frac{\partial}{\partial\mu}\left[\left(1-\mu^2\right)\frac{\kappa_{\theta\theta}}{r^2}\right]\right\} + \frac{\partial}{\partial p^3}\left(\frac{1}{r^2}\frac{\partial r^2 V}{\partial r}p^3 f\right) - \frac{1}{r^2}\frac{\partial}{\partial r}\left(r^2 V f\right). \tag{25}$$

[29] By setting $F = r^2 f$ [*Alanko-Huotari et al.*, 2007; *Bobik et al.*, 2008], equation (25) can be rewritten as

$$\frac{\partial F}{\partial t} = -\frac{\partial}{\partial r}(VF) - \frac{\partial}{\partial r}\left(F\frac{1}{r^2}\frac{\partial r^2\kappa_{rr}}{\partial r}\right) - \frac{\partial}{\partial\mu}\left\{F\frac{\partial}{\partial\mu}\left[\left(1-\mu^2\right)\frac{\kappa_{\theta\theta}}{r^2}\right]\right\} - \frac{\partial}{\partial p^3}\left(-\frac{1}{r^2}\frac{\partial r^2 V}{\partial r}p^3 F\right) + \frac{\partial}{\partial r}\frac{\partial}{\partial r}(\kappa_{rr}F) + \frac{\partial}{\partial\mu}\frac{\partial}{\partial\mu}\left[\left(1-\mu^2\right)\frac{\kappa_{\theta\theta}}{r^2}F\right]. \tag{26}$$

[30] In this case, setting

$$\mathbf{q} = \{r, \mu, p\}, \tag{27}$$

$$\mathbf{A} = \left\{\frac{1}{r^2}\frac{\partial r^2\kappa_{rr}}{\partial r} + V,\ \frac{\partial}{\partial\mu}\left[\frac{(1-\mu^2)\kappa_{\theta\theta}}{r^2}\right],\ -\frac{p}{3r^2}\frac{\partial r^2 V}{\partial r}\right\}, \tag{28}$$

$$\Delta\mathbf{W} = \sqrt{\Delta t}\{dw_r, dw_\mu, 0\}, \tag{29}$$

where $\Delta\mathbf{W}$ is a Wiener process given by the standard normal distribution with a mean of zero and a standard deviation of one and

$$\mathsf{B} = \begin{bmatrix} \sqrt{2\kappa_{rr}} & 0 & 0 \\ 0 & \frac{1}{r}\sqrt{2(1-\mu^2)\kappa_{\theta\theta}} & 0 \\ 0 & 0 & 0 \end{bmatrix}, \tag{30}$$

we find the corresponding SDEs for this transformation according to Ito's theorem are

$$\Delta r = \left(\frac{1}{r^2}\frac{\partial r^2\kappa_{rr}}{\partial r} + V\right)\Delta t + \sqrt{2\kappa_{rr}\Delta t}\,dw_r, \tag{31}$$

$$\Delta\mu = \frac{\partial}{\partial\mu}\left[\frac{(1-\mu^2)\kappa_{\theta\theta}}{r^2}\right]\Delta t + \frac{1}{r}\sqrt{2(1-\mu^2)\kappa_{\theta\theta}\Delta t}\,dw_\mu, \tag{32}$$

$$\Delta p = -\frac{p}{3r^2}\frac{\partial r^2 V}{\partial r}\Delta t. \tag{33}$$

[31] *Jokipii and Levy* [1977] used another formula, i.e., $F = \sin\theta r^2 f$. The corresponding FPE in this case is

$$\frac{\partial F}{\partial t} = \frac{\partial}{\partial r}\frac{\partial}{\partial r}(\kappa_{rr}F) - \frac{\partial}{\partial r}\left(F\frac{1}{r^2}\frac{\partial r^2\kappa_{rr}}{\partial r}\right) - \frac{\partial}{\partial r}(VF) + \frac{\partial}{\partial\theta}\frac{\partial}{\partial\theta}\left(\frac{\kappa_{\theta\theta}}{r^2}F\right) - \frac{\partial}{\partial\theta}\left(F\frac{1}{r^2\sin\theta}\frac{\partial\sin\theta\kappa_{\theta\theta}}{\partial\theta}\right) + \frac{\partial}{\partial p^3}\left(\frac{1}{r^2}\frac{\partial r^2 V}{\partial r}p^3 F\right). \tag{34}$$

[32] Similarly, the corresponding SDEs are

$$\Delta r = \left(\frac{1}{r^2}\frac{\partial r^2\kappa_{rr}}{\partial r} + V\right)\Delta t + \sqrt{2\kappa_{rr}\Delta t}\,dw_r, \tag{35}$$

$$\Delta\theta = \left(\frac{1}{r^2\sin\theta}\frac{\partial\sin\theta\kappa_{\theta\theta}}{\partial\theta}\right)\Delta t + \frac{1}{r}\sqrt{2\kappa_{\theta\theta}\Delta t}\,dw_\theta, \tag{36}$$

$$\Delta p = -\frac{p}{3r^2}\frac{\partial r^2 V}{\partial r}\Delta t. \tag{37}$$

[33] Actually, without explicitly using Ito's theorem, *Jokipii and Levy* [1977] immediately realize that transition moments satisfy the equations, $\langle\Delta r^2\rangle = 2\kappa_{rr}\Delta t$, $\langle\Delta\theta^2\rangle = 2\kappa_{\theta\theta}\Delta t/r^2$, $\langle\Delta r\rangle = (2\kappa_{rr}/r + V)\Delta t$, $\langle\Delta\theta\rangle = \kappa_{\theta\theta}\cot\theta\Delta t/r^2$, $\langle\Delta p\rangle = -2Vp\Delta t/3r$, which follows from a comparison of equation (34) with the FPE in the work by *Chandrasekhar* [1943, equation 223]. Therefore we can integrate the corresponding SDEs directly in polar coordinates without transforming them into Cartesian coordinates. See section 3 for more details.

[34] We have shown that there are two different sets of SDEs, according to different transformations in order to reach the standard form of FPE. However, it turns out that these two approaches yield the same results (see Figure 1 and section 3 for more details).

2.3. Three-Dimensional Stochastic Method

[35] For 3-D modulation of cosmic rays in the heliosphere, we consider three different scenarios for the comparison of the finite difference method and the stochastic method. The first one is 3-D without drift effects and $\boldsymbol{\kappa}$ with cross terms (such as $\kappa_{r\phi}$ [see, e.g., *Burger et al.*, 2008]) suppressed (see Figure 2). The transformation from field-aligned to heliocentric spherical coordinates, for a general

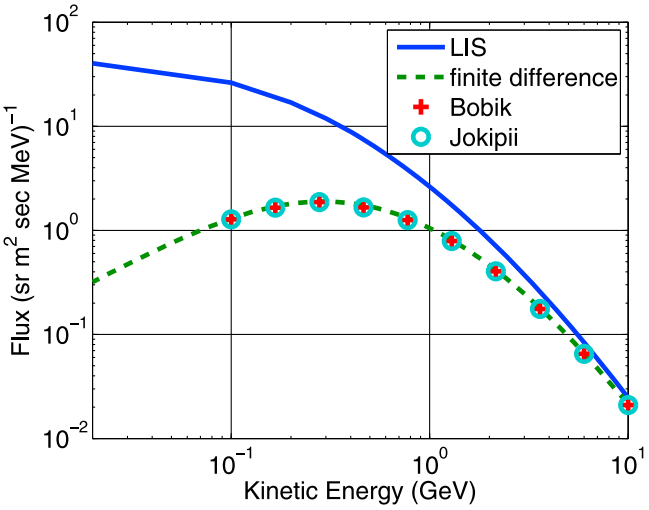

Figure 1. Benchmark for the 2-D steady state method. The solid line is the LIS. The dashed line denotes the finite difference method results [*Burger and Hattingh*, 1995]. The crosses denote results using *Bobik et al.*'s [2008] formulas (equations (31)–(33)), and the open circles denote results using *Jokipii and Levy*'s [1977] formulas (equations (35)–(37)).

three-dimensional form of the heliospheric magnetic field, is given by *Burger et al.* [2008]. The FPE in this case is

$$\frac{\partial f}{\partial t} = \frac{1}{r^2}\frac{\partial}{\partial r}\left(r^2\kappa_{rr}\frac{\partial f}{\partial r}\right) + \frac{1}{r^2\sin\theta}\frac{\partial}{\partial\theta}\left(\kappa_{\theta\theta}\sin\theta\frac{\partial f}{\partial\theta}\right) + \frac{1}{r^2\sin^2\theta}\frac{\partial}{\partial\phi}\cdot\left(\kappa_{\phi\phi}\frac{\partial f}{\partial\phi}\right) + \frac{1}{r^2}\frac{\partial}{\partial r}\left(r^2V\right)\frac{\partial}{\partial p^3}\left(p^3 f\right) - \frac{1}{r^2}\frac{\partial}{\partial r}\left(r^2 V f\right). \quad (38)$$

The corresponding SDEs are

$$\Delta r = \left(\frac{1}{r^2}\frac{\partial r^2\kappa_{rr}}{\partial r} + V\right)\Delta t + \sqrt{2\kappa_{rr}\Delta t}\,dw_r, \quad (39)$$

$$\Delta\theta = \frac{1}{r^2\sin\theta}\frac{\partial\sin\theta\kappa_{\theta\theta}}{\partial\theta}\Delta t + \frac{1}{r}\sqrt{2\kappa_{\theta\theta}\Delta t}\,dw_\theta, \quad (40)$$

$$\Delta\phi = \frac{1}{r^2\sin^2\theta}\frac{\partial\kappa_{\phi\phi}}{\partial\phi}\Delta t + \frac{1}{r\sin\theta}\sqrt{2\kappa_{\phi\phi}\Delta t}\,dw_\phi, \quad (41)$$

$$\Delta p = -\frac{p}{3r^2}\frac{\partial r^2 V}{\partial r}\Delta t. \quad (42)$$

[36] The second one is 3-D without drift effects but $\boldsymbol{\kappa}$ with cross terms. Here we assume $\kappa_{r\phi} = \kappa_{\phi r}$ and the order of all the derivatives are exchangeable.

$$\frac{\partial f}{\partial t} = \frac{1}{r^2}\frac{\partial}{\partial r}\left(r^2\kappa_{rr}\frac{\partial f}{\partial r}\right) + \frac{1}{r^2\sin\theta}\frac{\partial}{\partial\theta}\left(\kappa_{\theta\theta}\sin\theta\frac{\partial f}{\partial\theta}\right) + \frac{1}{r^2\sin^2\theta}\frac{\partial}{\partial\phi}\cdot\left(\kappa_{\phi\phi}\frac{\partial f}{\partial\phi}\right) + \frac{1}{r\sin\theta}\frac{\partial}{\partial\phi}\left(\kappa_{\phi r}\frac{\partial f}{\partial r}\right) + \frac{1}{r^2\sin\theta}\frac{\partial}{\partial r}\left(r\kappa_{r\phi}\frac{\partial f}{\partial\phi}\right) + \frac{1}{r^2}\frac{\partial}{\partial r}\left(r^2V\right)\frac{\partial}{\partial p^3}\left(p^3 f\right) - \frac{1}{r^2}\frac{\partial}{\partial r}\left(r^2 V f\right). \quad (43)$$

The corresponding SDEs are

$$\Delta r = \left(\frac{1}{r^2}\frac{\partial r^2\kappa_{rr}}{\partial r} + \frac{1}{r\sin\theta}\frac{\partial\kappa_{r\phi}}{\partial\phi} + V\right)\Delta t + [\mathsf{B}\cdot\Delta\mathbf{W}]_r, \quad (44)$$

$$\Delta\theta = \frac{1}{r^2\sin\theta}\frac{\partial\sin\theta\kappa_{\theta\theta}}{\partial\theta}\Delta t + [\mathsf{B}\cdot\Delta\mathbf{W}]_\theta, \quad (45)$$

$$\Delta\phi = \frac{1}{r^2\sin^2\theta}\frac{\partial\kappa_{\phi\phi}}{\partial\phi} + \frac{1}{r^2\sin\theta}\frac{\partial r\kappa_{r\phi}}{\partial r}\Delta t + [\mathsf{B}\cdot\Delta\mathbf{W}]_\phi, \quad (46)$$

$$\Delta p = -\frac{p}{3r^2}\frac{\partial r^2 V}{\partial r}\Delta t. \quad (47)$$

The calculation of B in this scenario is listed in the Appendix C.

[37] The last scenario is a fully 3-D model with drift effects and a fully 3-D $\boldsymbol{\kappa}$ tensor including cross terms (see Figures 3, 4, and 5). The general weak scattering drift velocity of a particle with charge q, momentum p, and speed v is given by *Jokipii et al.* [1977] for the case of a flat current sheet inside the equatorial plane,

$$\mathbf{V}_d = \frac{pv}{3q}\nabla\times\left(\frac{\mathbf{B}}{B^2}\right) = \frac{2pvr}{3qA(1+\gamma^2)^2}\left[1-2H\left(\theta-\frac{\pi}{2}\right)\right] \times\left[-\frac{\gamma}{\tan\theta}\hat{\mathbf{e}}_r + (2+\gamma^2)\gamma\hat{\mathbf{e}}_\theta + \frac{\gamma^2}{\tan\theta}\hat{\mathbf{e}}_\phi\right] + \frac{2pvr}{3qA(1+\gamma^2)} \cdot\delta\left(\theta-\frac{\pi}{2}\right)\left(\gamma\hat{\mathbf{e}}_r + \hat{\mathbf{e}}_\phi\right), \quad (48)$$

where $\gamma = r\Omega_\odot\sin\theta/V$. For the current sheet drift, we did not use the last term in the form given but adopted a formula following from a result by *Burger et al.* [1985] and *Burger* [1987] for the drift along the current sheet,

$$V_{dc} = \left(0.457 - 0.412\frac{|d|}{R_g} + 0.0915\frac{|d|^2}{R_g^2}\right)v, \quad (49)$$

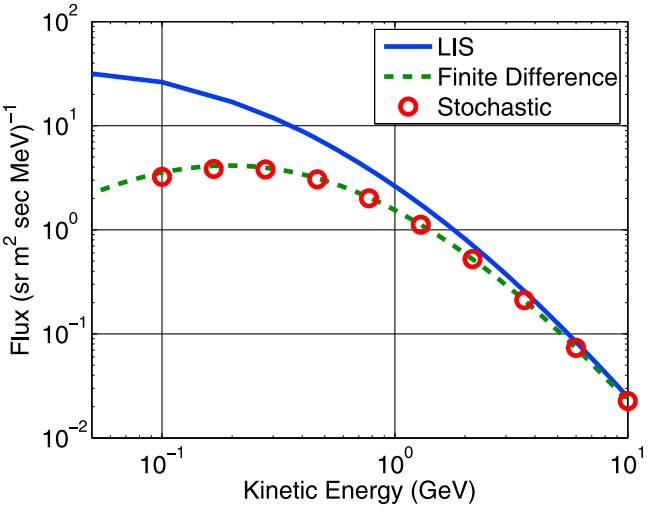

Figure 2. Benchmark for the 3-D steady state method for the first scenario of section 2.3 without drift and without cross terms in the diffusion tensor. The circles denote our stochastic results, and the dashed line denotes the our finite difference results.

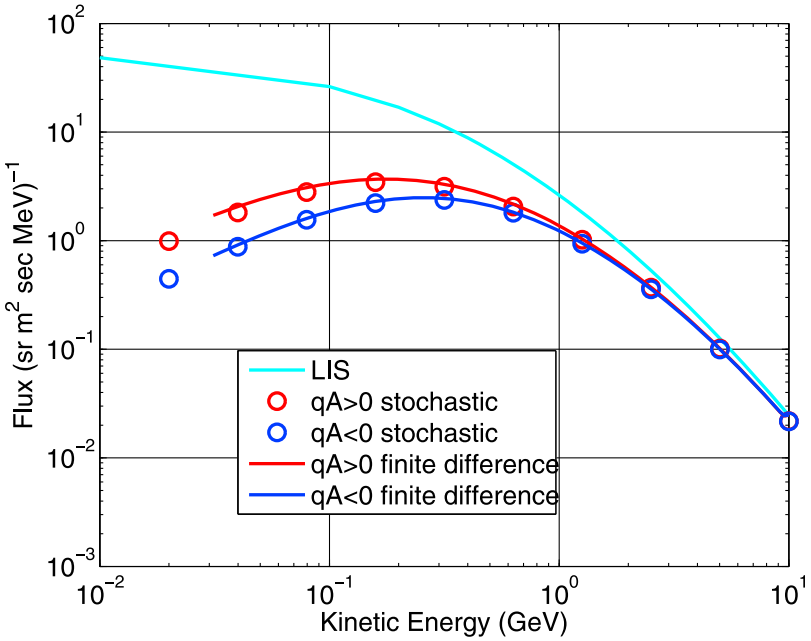

Figure 3. Benchmark for the 3-D steady state method for the third scenario in section 2.3 with $\kappa_{\|}$ specified by equation (4). As in Figure 2, the circles denote our stochastic results. Red and dark blue lines denote the our finite difference results. Red denotes the results for $qA > 0$, and dark blue denotes $qA < 0$.

where d is the distance to the current sheet and R_g is the Larmor radius. This formula is valid when d is smaller than 2 times R_g.

[38] Parker's transport equation in this case is

$$\frac{\partial f}{\partial t} = \frac{1}{r^2}\frac{\partial}{\partial r}\left(r^2\kappa_{rr}\frac{\partial f}{\partial r}\right) + \frac{1}{r^2\sin\theta}\frac{\partial}{\partial\theta}\left(\kappa_{\theta\theta}\sin\theta\frac{\partial f}{\partial\theta}\right) + \frac{1}{r^2\sin^2\theta}\frac{\partial}{\partial\phi}\left(\kappa_{\phi\phi}\frac{\partial f}{\partial\phi}\right) + \frac{1}{r\sin\theta}\frac{\partial}{\partial\phi}\left(\kappa_{\phi r}\frac{\partial f}{\partial r}\right) + \frac{1}{r^2\sin\theta}\frac{\partial}{\partial r}\left(r\kappa_{r\phi}\frac{\partial f}{\partial\phi}\right) + \frac{1}{r^2}\frac{\partial}{\partial r}\left(r^2V\right)\frac{\partial}{\partial p^3}\left(p^3 f\right) - \frac{1}{r^2}\frac{\partial}{\partial r}\left(r^2 V f\right) - \frac{1}{r^2}\frac{\partial}{\partial r}\left(r^2 V_{dr} f\right) - \frac{1}{r\sin\theta}\frac{\partial}{\partial\theta}\left(\sin\theta V_{d\theta} f\right) - \frac{1}{r\sin\theta}\frac{\partial}{\partial\phi}\left(V_{d\phi} f\right). \quad (50)$$

The corresponding SDEs are

$$\Delta r = \left(\frac{1}{r^2}\frac{\partial r^2\kappa_{rr}}{\partial r} + \frac{1}{r\sin\theta}\frac{\partial\kappa_{r\phi}}{\partial\phi} + V + V_{dr}\right)\Delta t + [\mathsf{B}\cdot\Delta\mathbf{W}]_r, \quad (51)$$

$$\Delta\theta = \frac{1}{r^2\sin\theta}\frac{\partial\sin\theta\kappa_{\theta\theta}}{\partial\theta}\Delta t + \frac{V_{d\theta}}{r}\Delta t + [\mathsf{B}\cdot\Delta\mathbf{W}]_\theta, \quad (52)$$

$$\Delta\phi = \frac{1}{r^2\sin^2\theta}\frac{\partial\kappa_{\phi\phi}}{\partial\phi} + \frac{1}{r^2\sin\theta}\frac{\partial r\kappa_{r\phi}}{\partial r}\Delta t + \frac{V_{d\phi}}{r\sin\theta}\Delta t + [\mathsf{B}\cdot\Delta\mathbf{W}]_\phi, \quad (53)$$

$$\Delta p = -\frac{p}{3r^2}\frac{\partial r^2 V}{\partial r}\Delta t. \quad (54)$$

The calculation of B can be done similarly as in the last scenario.

3. Benchmarks

3.1. Benchmarks for Steady State Solutions

[39] Because *Yamada et al.* [1998] already benchmarked the 1-D steady state solution with a Crank-Nicholson method, we start the benchmark with the 2-D steady state

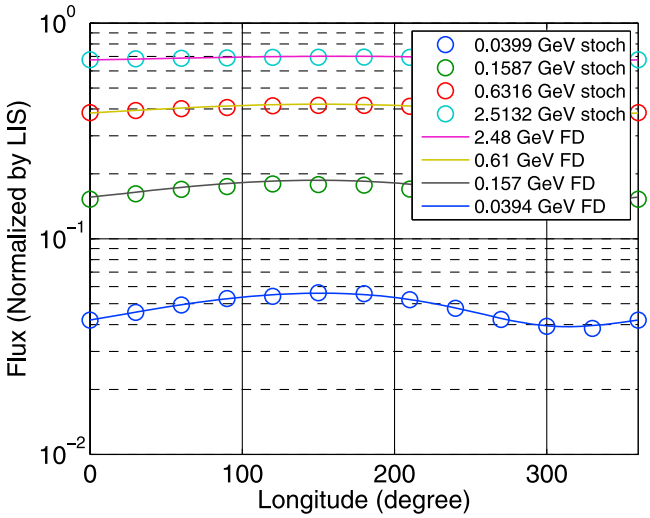

Figure 4. Benchmark for the 3-D steady state method for the last scenario in section 2.3 with $\kappa_{\|}$ specified by equation (5) and with $qA > 0$. As in Figure 3, the circles denote our stochastic (denoted by "stoch" in the legend) results, and the solid lines denote the our finite difference (FD) results.

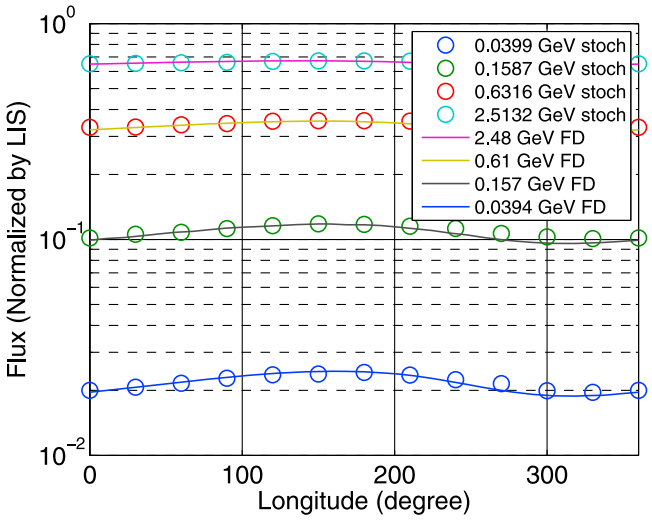

Figure 5. Benchmark for the 3-D steady state method for the last scenario in section 2.3 with $\kappa_{\|}$ specified by equation (5) and with $qA < 0$. As in Figure 3, the circles denote our stochastic results, and the solid lines denote the our finite difference results.

solution. The benchmarks for 2-D steady state results are shown in Figure 1. The solid line is the local interstellar spectrum (LIS). The dashed line denotes the finite difference method results [*Burger and Hattingh*, 1995]. The crosses denote results using the first formula equations (31)–(33) [*Bobik et al.*, 2008], and the open circles are for results using the second formula equations (35)–(37) [*Jokipii and Levy*, 1977]. Here we use equation (4) for κ with $\kappa_0 = 2 \times 10^{23}$ cm^{2}sec^{-1}GV^{-1}. Obviously, Figure 1 shows that these two different stochastic methods are in agreement. The reason for this is that the eigenvalues and the normalized eigenvectors for these SDEs are identical. Further the two stochastic approaches yield almost identical results to the finite difference method. We emphasize that these results are obtained by integrating the SDEs in polar coordinates, not in the Euclidean space. Therefore, this benchmark also validated our approach.

[40] The benchmark for 3-D steady state results are shown in Figures 2–5. Figure 2 is for the first scenario without drift and without cross terms in the diffusion tensor. The parallel diffusion coefficient $\kappa_{\|}$ is specified by equation (4), where $\kappa_0 = 1 \times 10^{22}$ cm^{2}sec^{-1}GV^{-1}. The LIS is denoted by the blue line in Figure 2. The finite difference method result is presented by the green dotted line, and the red open circles are our stochastic results. The agreement between these results is excellent (within 1%) for the two different methods.

[41] Figures 3–5 show the benchmark for the third scenario in section 2.3 (although not shown, we have performed benchmarks for the second scenario and many others). Figure 3 is for κ specified by equation (4). Figures 4 and 5 are for $\kappa_{\|}$ specified by equation (5). For both cases, $\kappa_0 = 1 \times 10^{22}$cm^{2}sec^{-1}GV^{-1} In Figure 3, for $qA > 0$, the relative difference between the stochastic result and the finite difference result is better than 10%. For qA < 0, the relative difference is better than 5%. Figures 4 and 5 are for a fully 3-D scenario. Here $\boldsymbol{\kappa}$ is also a function of azimuth ϕ, and we show the normalized intensity at different longitudes in this plot. The agreements are good for qA > 0 and for qA < 0. We observe that the highest value of $\kappa_{\|}$ in equation (5) is at azimuth $\phi = 90°$. However, the peak intensities in Figures 4 and 5 are shifted to values higher than 90° owing to the spiral structure of the Parker field.

3.2. Benchmarks for Time-Dependent Solutions

[42] So far all the benchmarks are for the steady state solutions taking advantage of the finite difference codes in our group. However, we don't have this luxury to benchmark the time-dependent stochastic method in this way. But for simpler problems, other tools, like Mathematica, can provide us accurate solutions. Thus we seek a way to benchmark our method by using Mathematica to solve a simpler diffusion equation without losing the generality.

[43] Because the SDEs for the steady state method and for the time-dependent method are exactly the same, the benchmarks for the steady state solutions are also the benchmarks for the first step, solving the SDEs, in the time-dependent method. Thus we only need to benchmark the second step, obtaining the spectrum from the probability function by using equation (12), for the time-dependent method. So we use our time-dependent method to solve simpler problems which Mathematica can provide solutions for us to benchmark the second step. In all the cases discussed in this section, we use an initial condition specified by equation (13). Physically, this corresponds to a situation in which the "heliosphere" is initially empty of cosmic rays, while the LIS illuminates the boundary. Our time-dependent solutions track how GCRs gradually fill the heliosphere with the passage of time if diffusion is the only process that occurs.

[44] The diffusion equation for the purpose of benchmarking is

$$\frac{\partial u}{\partial t} = \boldsymbol{\kappa} \cdot \boldsymbol{\nabla}^2 u, \tag{55}$$

where $\boldsymbol{\kappa} = \kappa_0 [1 + 0.8 \sin(\Omega_\odot t)]$.

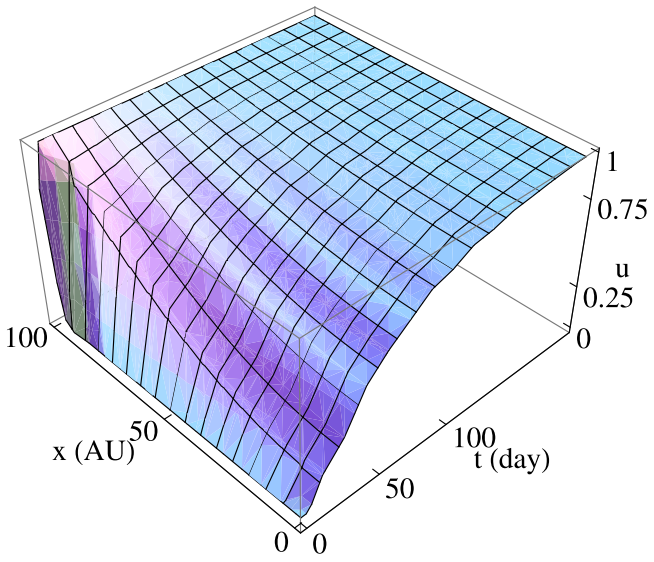

Figure 6. Mathematica solution for 1-D time-dependent diffusion with the reflecting inner boundary.

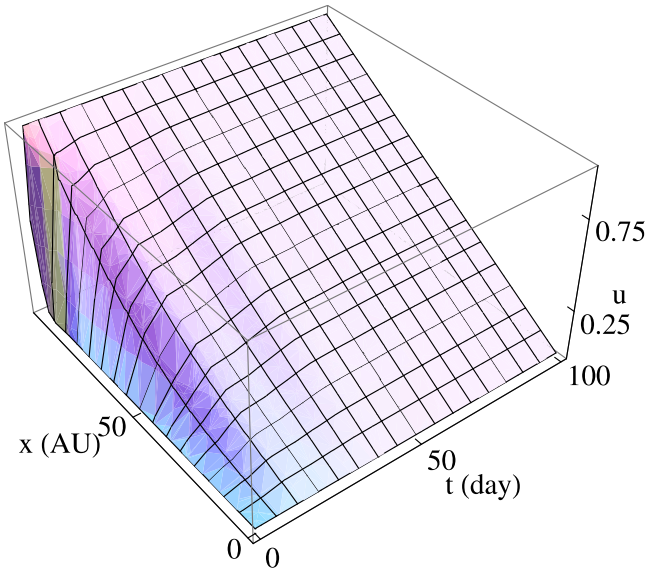

Figure 7. Mathematica solution for 1-D time-dependent diffusion with the absorbing inner boundary.

[45] Figure 6 shows the Mathematica 1-D solution for the reflecting inner boundary, $\partial u/\partial r = 0$ at $r = 0$, with time from 0 to 200 days. The outer boundary is specified as $u(100,t) = 1$. Figure 7 is the Mathematica 1-D solution for absorbing inner boundary, $u(0,t) = 0$, with time from 0 to 100 days. Other parameters are the same as those in Figure 6. These show the role of inner boundary condition is important in 1-D solutions. With the reflecting inner boundary, the heliosphere asymptotically becomes filled with cosmic rays at the level of the LIS, while for the absorbing inner boundary the asymptotic state is a uniform density gradient.

[46] The 1-D benchmarks are shown in Figures 8 and 9. The blue dotted line is the Mathematica 1-D solution. The open red circles denote our stochastic results for the reflecting inner boundary. The red dots denote our stochastic results for the absorbing inner boundary. Agreement is so good that the blue line is partially obscured by the stochastic (red) solution. Note that the scale of the y axis is different for the plots in Figures 8 and 9, which is the reason that the statistic behavior of our solution in Figure 9 is more evident. Especially for the reflecting boundary case, the 25.4 day period is clearly shown in both results.

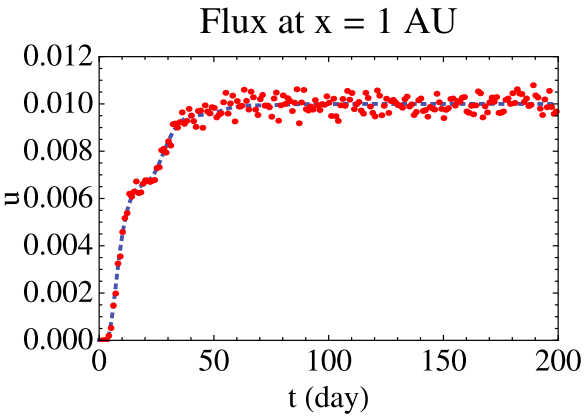

Figure 9. Benchmarks for 1-D time-dependent method with the absorbing inner boundary. The blue dotted line denotes the Mathematica solution with the same set of parameters. The red dots denote our stochastic results.

[47] The 2-D and 3-D benchmarks are shown in Figures 10 and 11. The blue lines denote the Mathematica solutions. The red circles denote our stochastic results. These are all for reflecting inner boundaries. To be specific, for 2-D diffusion, the boundary conditions are

$$\frac{\partial u}{\partial x}|_{x=0} = 0, \tag{56}$$

$$\frac{\partial u}{\partial y}|_{y=0} = 0, \tag{57}$$

$$u(100, y, t) = 1, \tag{58}$$

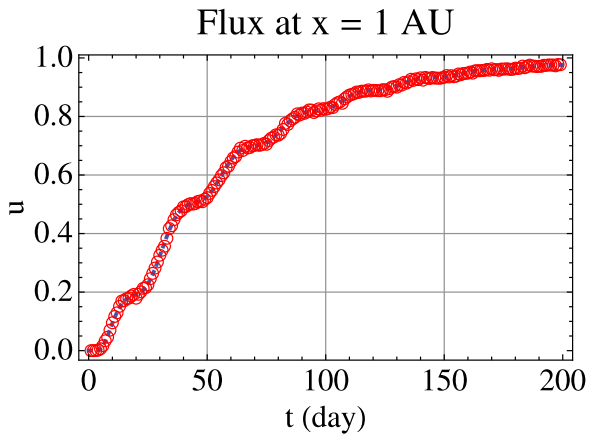

Figure 8. Benchmarks for 1-D time-dependent method with the reflecting inner boundary. The blue dotted line denotes the Mathematica solution with the same set of parameters. The open red circles denote our stochastic results.

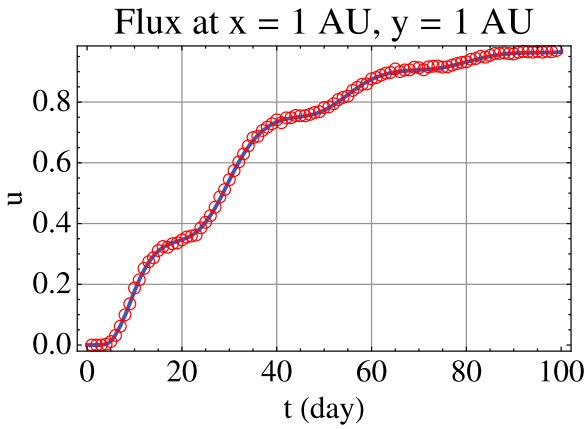

Figure 10. Benchmarks for 2-D time-dependent method with reflecting inner boundaries. The blue line denotes the Mathematica solution with the same set of parameters. The open red circles denote our stochastic results.

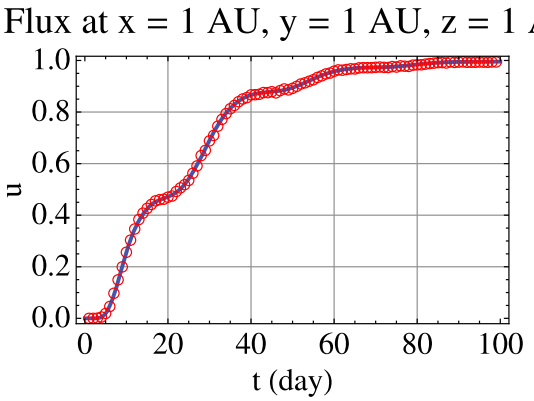

Figure 11. Benchmarks for 3-D time-dependent method with reflecting inner boundaries. As in Figure 10, the blue line denotes the Mathematica solution with the same set of parameters. The open red circles denote our stochastic results.

$$u(x, 100, t) = 1. \tag{59}$$

For 3-D, the boundary conditions are

$$\frac{\partial u}{\partial x}|_{x=0} = 0, \tag{60}$$

$$\frac{\partial u}{\partial y}|_{y=0} = 0, \tag{61}$$

$$\frac{\partial u}{\partial z}|_{z=0} = 0, \tag{62}$$

$$u(100, y, z, t) = 1, \tag{63}$$

$$u(x, 100, z, t) = 1, \tag{64}$$

$$u(x, y, 100, t) = 1. \tag{65}$$

The good agreement between our results with the Mathematica results proves that the second step in our time-dependent method is correct. Note that for the time needed to reach quasi-equilibrium for 1-D, 2-D, or 3-D is different in the reflecting inner boundary case. For 1-D, it takes about 200 days, 2-D about 100 days, and 3-D about 80 days. The computation time for a time-dependent solver in these benchmarks is several minutes on one CPU. To be more specific, let us take the 3-D case as an example, we employ 9000 particles for one energy level with the time step of 100 s. For a 100 day solution, which is the last point in Figure 11, the codes take about 7 min to finish on one of the CPUs of a dual-core INTEL E6850.

4. Conclusions and Future Work

[48] We present detailed benchmarks for our fully three-dimensional method for steady state solution as well as time-dependent solutions. For the steady state solutions, we show that the agreement between our stochastic results and the finite difference results is excellent. But our steady state method is different from any other 3-D method by using a different set of SDEs and by integrating the SDEs in spherical coordinates directly. Our steady state method can be viewed as an extension from *Jokipii and Levy* [1977] (2-D) to 3-D. For the time-dependent method, we benchmark it in two steps. The benchmarks for the steady state solution serve as the first step since the two methods use the exactly the same set of SDEs. The second step is done by employing Mathematica to solve a simple diffusion equation. As far as we know, our time-dependent method is the first of its kind. Although there are other time-dependent methods have been published, for example, by *Yamada et al.* [1999] and *Li et al.* [2009], they are time-dependent solvers only for one dimensional in space. Our method is also the only 3-D method that has been thoroughly benchmarked in the literature.

[49] This stochastic method is based on the assumption that each random process is independent of every other one. Therefore, it is suitable for parallel computing and distributed computing. Currently, our code is running in parallel. To use more idle computer resources, distributed computing is promising too. Also important is that almost 100 percent of the code can be parallelized which means we can speed up the calculation more significantly. With the advantage of using parallel computing and distributed computing, we believe a new era for the stochastic method has dawned.

Appendix A: Wiener Process

[50] In the stochastic equations, $\Delta\mathbf{W}$ satisfies a Wiener (also called Wiener-Lévy) process, which is a nonstationary Markov process that has a Gaussian distribution [see, e.g., *Gardiner*, 2004]

$$p(\mathbf{W}(t), t|\mathbf{W}(t_0), t_0) = \frac{1}{\sqrt{2\pi(t - t_0)}} e^{-[W_i(t) - W_i(t_0)]^2/2/(t-t_0)}, \tag{A1}$$

or equivalently

$$p(\Delta W_i) = \frac{1}{\sqrt{2\pi\Delta t}} e^{-\Delta W_i^2/2/\Delta t}. \tag{A2}$$

[51] What we use in our calculation is a normalized Gaussian distribution with a mean of zero and a standard deviation of one,

$$p(\Delta w_i) = \frac{1}{\sqrt{2\pi}} e^{-\Delta w_i^2/2}. \tag{A3}$$

It is easily shown that a Wiener process is self-similar in the sense that

$$\Delta W_i(\Delta t) = \lambda^{-1/2} \Delta W_i(\lambda \Delta t), \tag{A4}$$

and consequently

$$\Delta W_i(\Delta t) = \sqrt{\Delta t}\Delta w_i. \tag{A5}$$

Appendix B: General Form of Matrix B in 3-D

[52] The general form of the matrix B satisfies

$$\mathsf{B}\mathsf{B}^T = \begin{bmatrix} 2\kappa_{rr} & \frac{2\kappa_{r\theta}}{r} & \frac{2\kappa_{r\phi}}{r\sin\theta} \\ \frac{2\kappa_{r\theta}}{r} & \frac{2\kappa_{\theta\theta}}{r^2} & \frac{2\kappa_{\theta\phi}}{r^2\sin\theta} \\ \frac{2\kappa_{r\phi}}{r\sin\theta} & \frac{2\kappa_{\theta\phi}}{r^2\sin\theta} & \frac{2\kappa_{\phi\phi}}{r^2\sin^2\theta} \end{bmatrix}. \tag{B1}$$

The real B exists if Matrix B1 is positive definite, and this is true since the diffusion coefficients parallel and perpendicular to the background field are positive by definition. For a general field with a meridional component, like Fisk-type fields [*Fisk*, 1996; *Burger and Hitge*, 2004], a possibility for B is

$$\begin{bmatrix} \sqrt{\frac{\kappa_{\phi\phi}\kappa_{r\theta}^2 - 2\kappa_{r\phi}\kappa_{r\theta}\kappa_{\theta\phi} + \kappa_{rr}\kappa_{\theta\phi}^2 + \kappa_{\theta\theta}\kappa_{r\phi}^2 - \kappa_{rr}\kappa_{\theta\theta}\kappa_{\phi\phi}}{0.5\left(\kappa_{\theta\phi}^2 - \kappa_{\theta\theta}\kappa_{\phi\phi}\right)}} & \frac{\kappa_{r\phi}\kappa_{\theta\phi} - \kappa_{r\theta}\kappa_{\phi\phi}}{\kappa_{\theta\phi}^2 - \kappa_{\theta\theta}\kappa_{\phi\phi}}\sqrt{\left(2\kappa_{\theta\theta} - \frac{2\kappa_{\theta\phi}^2}{\kappa_{\phi\phi}}\right)} & \frac{\sqrt{2}\kappa_{r\phi}}{\sqrt{\kappa_{\phi\phi}}} \\ 0 & \frac{\sqrt{2\left(\kappa_{\theta\theta} - \kappa_{\theta\phi}^2/\kappa_{\phi\phi}\right)}}{r} & \frac{\kappa_{\theta\phi}}{r}\sqrt{\frac{2}{\kappa_{\phi\phi}}} \\ 0 & 0 & \frac{\sqrt{2\kappa_{\phi\phi}}}{r\sin\theta} \end{bmatrix},$$

which means that our method in this paper mainly for Parker field can be extended for other heliospheric magnetic fields.

[53] For Parker-type fields, without a meridional component and consequently $\kappa_{r\theta} = \kappa_{\theta\phi} = 0$, B can be simplified to

$$\mathsf{B} = \begin{bmatrix} \sqrt{2\kappa_{rr} - \frac{2\kappa_{r\phi}^2}{\kappa_{\phi\phi}}} & 0 & \frac{\sqrt{2}\kappa_{r\phi}}{\sqrt{\kappa_{\phi\phi}}} \\ 0 & \frac{\sqrt{2\kappa_{\theta\theta}}}{r} & 0 \\ 0 & 0 & \frac{\sqrt{2\kappa_{\phi\phi}}}{r\sin\theta} \end{bmatrix}. \tag{B2}$$

This matrix is not unique and an alternative as used in this paper is given in Appendix C.

Appendix C: Matrix B for Parker Field

[54] To determine the matrix, B, in equations (44)–(47), we need to decompose the following matrix D,

$$\mathsf{B}\mathsf{B}^T = \begin{bmatrix} 2\kappa_{rr} & 0 & \frac{2\kappa_{r\phi}}{r\sin\theta} \\ 0 & \frac{2\kappa_{\theta\theta}}{r^2} & 0 \\ \frac{2\kappa_{\phi r}}{r\sin\theta} & 0 & \frac{2\kappa_{\phi\phi}}{r^2\sin^2\theta} \end{bmatrix},$$

into a product of two matrices, such as $\mathsf{D} = \mathsf{B}\mathsf{B}^T$.

[55] Since this matrix is positive definite and symmetric, the eigenvalues of this matrix are positive. The eigenvalues are

$$\boldsymbol{\lambda} = \begin{bmatrix} \kappa_{rr} + \frac{\kappa_{\phi\phi}}{r^2\sin^2\theta} - \sqrt{\left(\frac{\kappa_{\phi\phi}}{r^2\sin^2\theta} - \kappa_{rr}\right)^2 + \left(\frac{2\kappa_{r\phi}}{r\sin\theta}\right)^2} \\ \frac{2\kappa_{\theta\theta}}{r^2} \\ \kappa_{rr} + \frac{\kappa_{\phi\phi}}{r^2\sin^2\theta} + \sqrt{\left(\frac{\kappa_{\phi\phi}}{r^2\sin^2\theta} - \kappa_{rr}\right)^2 + \left(\frac{2\kappa_{r\phi}}{r\sin\theta}\right)^2} \end{bmatrix}.$$

If we define

$$\begin{aligned} a &= \kappa_{rr} - \frac{\kappa_{\phi\phi}}{r^2\sin^2\theta}, \\ b &= \frac{2\kappa_{r\phi}}{r\sin\theta}, \\ c &= \kappa_{rr} + \frac{\kappa_{\phi\phi}}{r^2\sin^2\theta}, \end{aligned}$$

the corresponding eigenvectors are,

$$\begin{bmatrix} \frac{1}{b}\left(a - \sqrt{a^2+b^2}\right) & 0 & \frac{1}{b}\left(a - \sqrt{a^2+b^2}\right) \\ 0 & 1 & 0 \\ 1 & 0 & 1 \end{bmatrix}. \tag{C1}$$

Thus the matrix B is

$$\begin{bmatrix} \frac{\alpha}{b}\left(a - \sqrt{a^2+b^2}\right)\sqrt{c - \sqrt{a^2+b^2}} & 0 & \frac{\beta}{b}\left(a + \sqrt{a^2+b^2}\right)\sqrt{c + \sqrt{a^2+b^2}} \\ 0 & 1 & 0 \\ \alpha\sqrt{c - \sqrt{a^2+b^2}} & 0 & \beta\sqrt{c + \sqrt{a^2+b^2}} \end{bmatrix}, \tag{C2}$$

where α and β come from the normalization of the eigenvectors.

[56] By setting

$$\mathbf{q} = \{r, \theta, \phi, p\}, \tag{C3}$$

$$\mathbf{A} = \left\{ \frac{1}{r^2}\frac{\partial r^2 \kappa_{rr}}{\partial r} + \frac{1}{r\sin\theta}\frac{\partial \kappa_{r\phi}}{\partial \phi} + V + v_{dr}, \frac{1}{r^2\sin\theta}\frac{\partial \sin\theta \kappa_{\theta\theta}}{\partial \theta} + \frac{v_{d\theta}}{r}, \right.$$
$$\left. \frac{1}{r^2\sin^2\theta}\frac{\partial \kappa_{\phi\phi}}{\partial \phi} + \frac{1}{r^2\sin\theta}\frac{\partial r\kappa_{r\phi}}{\partial r} + \frac{v_{d\phi}}{r\sin\theta}, -\frac{p}{3r^2}\frac{\partial r^2 V}{\partial r} \right\}, \tag{C4}$$

$$\Delta\mathbf{W} = \sqrt{\Delta t}\{dw_r, dw_\theta, dw_\phi, 0\}, \tag{C5}$$

we obtain the equations (44)–(47). The procedures to calculate matrix B for equations (51)–(54) are similar.

[57] **Acknowledgments.** This work was supported in part by NASA Guest Investigator grant NNX07AH73G, NASA Heliophysics Theory grant NNX08AI47G, the Charged Sign Dependence grant NNG05WC08G, and the South African National Research Foundation. R. A. Burger thanks I. Burger for many useful discussions on SDEs.

[58] Philippa Browning thanks the reviewers for their assistance in evaluating this manuscript.

References

Alanko-Huotari, K., I. G. Usoskin, K. Mursula, and G. A. Kovaltsov (2007), Stochastic simulation of cosmic ray modulation including a wavy heliospheric current sheet, *J. Geophys. Res.*, *112*, A08101, doi:10.1029/2007JA012280.

Alanko-Huotari, K., I. G. Usoskin, K. Mursula, and G. A. Kovaltsov (2009), Correction to "Stochastic simulation of cosmic ray modulation including a wavy heliospheric current sheet," *J. Geophys. Res.*, *114*, A03101, doi:10.1029/2008JA013919.

Ball, B., M. Zhang, H. Rassoul, and T. Linde (2005), Galactic cosmic-ray modulation using a solar minimum MHD heliosphere: A stochastic particle approach, *Astrophys. J.*, *634*, 1116–1125.

Bieber, J. W., R. A. Burger, R. Engel, T. K. Gaisser, S. Roesler, and T. Stanev (1999), Antiprotons at solar saximum, *Phys. Rev. Lett.*, *83*, 674–677.

Bobik, P., K. Kudela, M. Boschini, D. Grandi, M. Gervasi, and P. G. Rancoita (2008), Solar modulation model with reentrant particles, *Adv. Space Res.*, *41*, 339–342.

Burger, R. A. (1987), On the theory and application of drift motion of charged particles in inhomogeneous magnetic fields, Ph.D. thesis, Potchefstroomse Univ. vir Christelike Hoër Onderwys, Potchefstroomse, South Africa.

Burger, R. A., and M. Hattingh (1995), Steady-state drift-dominated modulation models for galactic cosmic rays, *Astrophys. Space Sci.*, *230*, 375–382.

Burger, R. A., and M. Hitge (2004), The effect of a fisk-type heliospheric magnetic field on cosmic-ray modulation, *Astrophys. J.*, *617*, L73–L76.

Burger, R. A., H. Moraal, and G. M. Webb (1985), Drift theory of charged particles in electric and magnetic fields, *Astrophys. Space Sci.*, *116*, 107–129.

Burger, R. A., T. P. J. Krüger, M. Hitge, and N. E. Engelbrecht (2008), A fisk-parker hybrid heliospheric magnetic field with a solar-cycle dependence, *Astrophys. J.*, *674*, 511–519.

Chandrasekhar, S. (1943), Stochastic problems in physics and astronomy, *Rev. Mod. Phys.*, *15*, 1–89.

Dröge, W., Y. Y. Kartavykh, B. Klecker, and G. A. Kovaltsov (2010), Anisotropic three-dimensional focused transport of solar energetic particles in the inner heliosphere, *Astrophys. J.*, *709*, 912–919.

Fisk, L. A. (1996), Motion of the footpoints of heliospheric magnetic field lines at the Sun: Implications for recurrent energetic particle events at high heliographic latitudes, *J. Geophys. Res.*, *101*, 15,547–15,554.

Gardiner, C. W. (2004), *Handbook of Stochastic Methods for Physics, Chemistry and the Natural Sciences*, 3rd ed., Springer, Berlin.

Gervasi, M., P. G. Rancoita, I. G. Usoskin, and G. A. Kovaltsov (1999), Monte-Carlo approach to galactic cosmic ray propagation in the heliosphere, *Nucl. Phys. B Proc. Suppl.*, *78*, 26–31.

Jokipii, J. R., and D. A. Kopriva (1979), Effects of particle drift on the transport of cosmic rays. III. Numerical models of galactic cosmic-ray modulation, *Astrophys. J.*, *234*, 384–392.

Jokipii, J. R., and E. H. Levy (1977), Effects of particle drifts on the solar modulation of galactic cosmic rays, *Astrophys. J.*, *213*, L85–L88.

Jokipii, J. R., and A. J. Owens (1975), Implications of observed charge states of low-energy solar cosmic rays, *J. Geophys. Res.*, *80*, 1209–1212.

Jokipii, J. R., and E. N. Parker (1970), On the convection, diffusion, and adiabatic deceleration of cosmic rays in the solar wind, *Astrophys. J.*, *160*, 735–744.

Jokipii, J. R., E. H. Levy, and W. B. Hubbard (1977), Effects of particle drift on cosmic-ray transport. I. General properties, application to solar modulation, *Astrophys. J.*, *213*, 861–868.

Kocharov, L., R. Vainio, G. A. Kovaltsov, and J. Torsti (1998), Adiabatic deceleration of solar energetic particles as deduced from Monte Carlo simulations of interplanetary transport, *Solar Phys.*, *182*, 195–215.

Kóta, J. (1977), Energy loss in the solar system and modulation of cosmic radiation, *Contrib. Int. Cosmic Ray Conf. IUPAP 15th*, vol. 11, 186–191.

Kóta, J., and J. R. Jokipii (1983), Effects of drift on the transport of cosmic rays. VI. A three-dimensional model including diffusion, *Astrophys. J.*, *265*, 573–581.

Li, G., et al. (2009), Modeling the transport of cosmic ray due to long-term variation using a stochastic differential method, paper presented at 31st International Cosmic Ray Conference, Univ. of Łódź, Łódź, Poland, 7–15 Jul.

Mewaldt, R. A., et al. (2009), Galactic cosmic ray intensities reach record levels in 2009, *Eos Trans. AGU*, *90*(52), Fall Meet. Suppl., Abstract SH13C-08.

Mitchell, J. W., et al. (2008), Solar modulation of low-energy antiproton and proton spectra measured by BESS, in *Proceedings of the 30th International Cosmic Ray Conference*, vol. 1, edited by R. Caballero et al., pp. 455–458, Univ. Nac. Auton. de Mexico, Mexico City.

Miyake, S., and S. Yanagita (2005), Effects of the tilted and wavy current sheet on the solar modulation of galactic cosmic rays, in *Proceedings of the 29th International Cosmic Ray Conference*, vol. 2, pp. 101–106, Tate Inst. of Fundame. Res., Mumbai, India.

Parker, E. N. (1965), The passage of energetic charged particles through interplanetary space, *Planet. Space Sci.*, *13*, 9–49.

Pei, C., J. R. Jokipii, and J. Giacalone (2006), Effect of a random magnetic field on the onset times of solar particle events, *Astrophys. J.*, *641*, 1222–1226.

Pei, C., J. W. Bieber, R. A. Burger, J. Clem, and W. H. Matthaeus (2009), On a stochastic approach to cosmic-ray modulation, paper presented at 31st International Cosmic Ray Conference, Univ. of Łódź, Łódź, Poland, 7–15 Jul.

Pei, C., J. W. Bieber, B. Breech, R. A. Burger, J. Clem, and W. H. Matthaeus (2010), Cosmic ray diffusion tensor throughout the heliosphere, *J. Geophys. Res.*, *115*, A03103, doi:10.1029/2009JA014705.

Potgieter, M. S., and H. Moraal (1985), A drift model for the modulation of galactic cosmic rays, *Astrophys. J.*, *294*, 425–440.

Roelof, E. C. (1969), Propagation of solar cosmic rays in the interplanetary magnetic field, in *Lectures in High-Energy Astrophysics, NASA SP-199*, edited by H. Ögelman and J. R. Wayland, pp. 111–135, Sci. and Tech. Inf. Div., NASA, Washington, D. C.

Webb, G. M., and L. J. Gleeson (1977), Green's theorem and Green's functions for the steady-state cosmic-ray equation of transport, *Astrophys. Space Sci.*, *50*, 205–223.

Webber, W. R., and P. R. Higbie (2003), Production of cosmogenic Be nuclei in the Earth's atmosphere by cosmic rays: Its dependence on solar modulation and the interstellar cosmic ray spectrum, *J. Geophys. Res.*, *108*(A9), 1355, doi:10.1029/2003JA009863.

Yamada, Y., S. Yanagita, and T. Yoshida (1998), A stochastic view of the solar modulation phenomena of cosmic rays, *Geophys. Res. Letters*, *25*, 2353–2356.

Yamada, Y., S. Yanagita, and T. Yoshida (1999), A stochastic simulation method for the solar cycle modulation of cosmic rays, *Adv. Space Res.*, *23*, 505–508.

Zhang, M. (1999a), A path integral approach to the theory of heliospheric cosmic-ray modulation, *Astrophys. J.*, *510*, 715–725.

Zhang, M. (1999b), A Markov stochastic process theory of cosmic-ray modulation, *Astrophys. J.*, *513*, 409–420.

Zhang, M., G. Qin, and H. Rassoul (2009), Propagation of solar energetic particles in three-dimensional interplanetary magnetic fields, *Astrophys. J.*, *692*, 109–132.

J. W. Bieber, J. Clem, and C. Pei, Bartol Research Institute, Department of Physics and Astronomy, University of Delaware, 217 Sharp Lab., Newark, DE 19716, USA. (jwbieber@bartol.udel.edu; clem@bartol.udel.edu; pei@bartol.udel.edu)

R. A. Burger, Unit for Space Physics, School of Physics, Private Bag X6001, North-West University, Potchefstroom Campus, Potchefstroom, 2520 South Africa. (adri.burger@nwu.ac.za)